

# Gradient-Based Predictive Pulse Pattern Control

Mirza Abdul Waris Begh, *Student Member, IEEE*, Petros Karamanakos, *Senior Member, IEEE*,  
and Tobias Geyer, *Senior Member, IEEE*

**Abstract**—This paper presents a control scheme that combines the optimal steady-state performance of optimized pulse patterns (OPPs) with the fast dynamics of direct model predictive control (MPC). Due to inherent challenges that relate to the utilization of OPPs in a closed-loop setting, OPPs are traditionally used in slow control loops. As a result, the associated dynamic performance of the drive system is considerably poor. To overcome this, in this work, a direct MPC algorithm is employed to manipulate the OPPs in a fast, yet optimal, manner. Specifically, the MPC algorithm takes advantage of the knowledge of the stator current evolution—as described by its gradient—within the prediction horizon. Subsequently, a constrained optimization problem with a receding horizon is solved to compute the optimal modification of the offline-computed OPP such that superior steady-state and dynamic performance is achieved. The effectiveness of the proposed method is verified based on a variable speed drive system, which consists of a two-level inverter and a low-voltage induction machine.

## I. INTRODUCTION

Among the control strategies used in power electronics, model predictive control (MPC) [1] has gained a lot of popularity due to its various advantages, including the ability to handle multiple control variables and system constraints [2]–[4]. From the several variants of MPC, direct MPC with reference tracking—also known as finite control set MPC (FCS-MPC)—has been widely used due to its simple design procedure and straightforward implementation [4]. Direct MPC exploits the finite number of possible switch positions of a power converter and allows the combination of the control and modulation problems into one computational stage [5]. However, due to the lack of a modulator, it suffers from a variable switching frequency and a non-discrete current harmonic spectrum, while its performance can be worse than that of conventional control and modulation methods if poorly designed [6]. Various solutions have been proposed to overcome these limitations, such as indirect MPC [7], i.e., MPC with modulator, or direct MPC with an implicit modulator. Examples of the latter include MPC with programmed pulse width modulation (PWM), such as optimized pulse patterns (OPPs) [8], and MPC with variable switching time instants, e.g., gradient-based MPC [9].

OPPs, in particular, are an attractive option since they produce minimal current harmonic distortion for a given switching frequency [8], [10]. More specifically, OPPs are calculated offline by solving an optimization problem that computes the switching angles of a given pulse pattern with quarter- and half-wave symmetry properties such that the minimum

current total harmonic distortion (THD) results. This procedure is performed for different pulse numbers, i.e., single-phase switch transitions over a quarter of the fundamental period, and modulation indices. In doing so, operation at a fixed switching frequency—which is an integer multiple of the fundamental—and a deterministic harmonic spectrum are achieved. Since OPPs are computed assuming steady-state operating conditions, when applied to a converter, the best possible steady-state performance is realized in terms of current THD [11]. However, using OPPs with a fast controller is a challenging task, implying that when employed in a closed-loop setting poor dynamic performance results. MPC with OPPs is therefore quite appealing since it can take advantage of the excellent steady-state performance and low current distortions attributed to OPPs as well as the fast dynamic responses during transients that can be achieved with MPC.

In this direction, [12] proposed a controller based on a stator current trajectory tracking approach. In this method, the steady-state current trajectory is derived based on the OPP in use and it is ensured that the actual current vector follows it. As an alternative, [13] proposed a controller using stator flux trajectory. Although this control method offers good performance, it requires a complicated observer structure to reconstruct the flux quantities. Moreover, these control schemes do not employ a receding horizon that provides feedback and enhances their robustness. On the other hand, [14] and [15] fully exploit the benefits of OPPs and MPC. Specifically, the stator currents have very low harmonic distortions—and as close to their theoretical minimum as possible—while the dynamic performance is on par with that of high-bandwidth controllers such as direct torque control (DTC) [16]. Extension of this method, however, to more complex systems and multiple control objectives is not straightforward.

Motivated by the above, an OPP-based MPC algorithm—named gradient-based predictive pulse pattern control (GP<sup>3</sup>C)—is proposed in this paper that, similar to [9], utilizes the gradients of the controlled variables. By *directly* manipulating the switching time instants of the offline-computed nominal OPP in use, favorable steady-state and dynamic operation are achieved. Moreover, formulating the optimization problem underlying MPC based on the gradients of the controlled variables equips the controller with high versatility and modularity. To highlight the potential of the proposed method, a low-voltage drive system consisting of a two-level voltage source inverter and an induction machine serves as a simple case study.

## II. DRIVE SYSTEM

Throughout this paper the quantities are normalized and presented in the per unit (p.u.) system. The modeling of the

M. A. W. Begh and P. Karamanakos are with the Faculty of Information Technology and Communication Sciences, Tampere University, 33101 Tampere, Finland; e-mail: mirza.begh@tuni.fi, p.karamanakos@ieee.org

T. Geyer is with ABB System Drives, 5300 Turgi, Switzerland; e-mail: t.geyer@ieee.org

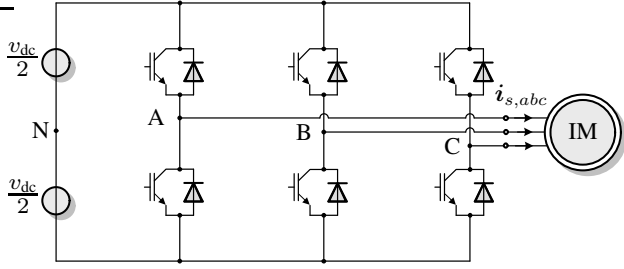


Fig. 1: Two-level three-phase voltage source inverter driving an IM.

drive system and the formulation of the control problem are carried out in the stationary orthogonal  $\alpha\beta$ -frame. Therefore, any variable in the  $abc$ -plane  $\xi_{abc} = [\xi_a \ \xi_b \ \xi_c]^T$  is transformed to a two-dimensional vector  $\xi_{\alpha\beta} = [\xi_\alpha \ \xi_\beta]^T$  in the  $\alpha\beta$ -plane<sup>1</sup> via the operation  $\xi_{\alpha\beta} = \mathbf{K}\xi_{abc}$ , where  $\mathbf{K}$  is

$$\mathbf{K} = \frac{2}{3} \begin{bmatrix} 1 & -\frac{1}{2} & -\frac{1}{2} \\ 0 & \frac{\sqrt{3}}{2} & -\frac{\sqrt{3}}{2} \end{bmatrix}.$$

As an illustrative example of a low-voltage variable speed drive system, consider a two-level inverter with the instantaneous (i.e., non-constant) dc-link voltage  $v_{dc}$  (with average value  $V_{dc}$ ) driving an induction machine (IM), as shown in Fig. 1. The output voltage of each phase can be  $-v_{dc}/2$  or  $v_{dc}/2$  depending on the *single-phase* switch position  $u_x \in \{-1, 1\}$ , with  $x \in \{a, b, c\}$ . As a result, the voltage applied to the stator terminals  $\mathbf{v}_s$ , is given as

$$\mathbf{v}_s = \frac{v_{dc}}{2} \mathbf{u} = \frac{v_{dc}}{2} \mathbf{K} \mathbf{u}_{abc}, \quad (1)$$

where  $\mathbf{u}_{abc} = [u_a \ u_b \ u_c]^T \in \{-1, 1\}^3$  is the three-phase switch position.

Considering the squirrel-cage induction machine, its dynamics can be described based on the stator current  $\mathbf{i}_s$ , the rotor flux  $\psi_r$  and the angular speed of the rotor  $\omega_r$ , i.e., [17]

$$\frac{d\mathbf{i}_s}{dt} = -\frac{1}{\tau_s} \mathbf{i}_s + \left( \frac{1}{\tau_r} \mathbf{I}_2 - \omega_r \begin{bmatrix} 0 & -1 \\ 1 & 0 \end{bmatrix} \right) \frac{X_m}{\Phi} \psi_r + \frac{X_r}{\Phi} \mathbf{v}_s \quad (2a)$$

$$\frac{d\psi_r}{dt} = \frac{X_m}{\tau_r} \mathbf{i}_s - \frac{1}{\tau_r} \psi_r + \omega_r \begin{bmatrix} 0 & -1 \\ 1 & 0 \end{bmatrix} \psi_r \quad (2b)$$

$$\frac{d\omega_r}{dt} = \frac{1}{H} (T_e - T_\ell), \quad (2c)$$

where  $R_s$  ( $R_r$ ) is the stator (rotor) resistance,  $X_{ls}$  ( $X_{lr}$ ) and  $X_m$  the stator (rotor) leakage and mutual reactances, respectively. The moment of inertia is denoted by  $H$ , while  $T_e$  and  $T_\ell$  are the electromagnetic and mechanical load torque, respectively. Moreover,  $\tau_s = X_r \Phi / (R_s X_r^2 + R_r X_m^2)$  and  $\tau_r = X_r / R_r$  are the stator and rotor transient time constants, respectively, while the constant  $\Phi$  is defined as  $\Phi = X_s X_r - X_m^2$ , with  $X_s = X_{ls} + X_m$  and  $X_r = X_{lr} + X_m$ . Finally,  $\mathbf{I}_2$  is a two-dimensional identity matrix.

From (1) and (2), the continuous-time state-space model of

<sup>1</sup>Hereafter, all variables in the  $abc$ -plane are denoted by their corresponding subscript, whereas the subscript is omitted for those in the  $\alpha\beta$ -plane to simplify the notation.

the drive system is written as

$$\frac{d\mathbf{x}(t)}{dt} = \mathbf{F}\mathbf{x}(t) + \mathbf{G}\mathbf{u}_{abc}(t) \quad (3a)$$

$$\mathbf{y}(t) = \mathbf{C}\mathbf{x}(t), \quad (3b)$$

where  $\mathbf{x} = [i_{s\alpha} \ i_{s\beta} \ \psi_{r\alpha} \ \psi_{r\beta}]^T \in \mathbb{R}^4$  and  $\mathbf{y} = [i_{s\alpha} \ i_{s\beta}]^T \in \mathbb{R}^2$  are the state and output vectors, respectively, and the three-phase switch position  $\mathbf{u}_{abc}$  is the input vector. Moreover,  $\mathbf{F} \in \mathbb{R}^{4 \times 4}$ ,  $\mathbf{G} \in \mathbb{R}^{4 \times 3}$ , and  $\mathbf{C} \in \mathbb{R}^{2 \times 4}$  are the system, input and output matrices, respectively, which characterize the system and can be derived using (2), see [5, Appendix 5.A]. Note that, compared with  $\mathbf{i}_s$  and  $\psi_r$ ,  $\omega_r$  changes slowly, thus it is not considered as state of the drive model, but rather a (slowly) varying parameter.

Using exact discretization with a sampling interval  $T_s$ , the discrete-time state-space model of the system (3) becomes

$$\mathbf{x}(k+1) = \mathbf{A}\mathbf{x}(k) + \mathbf{B}\mathbf{u}_{abc}(k) \quad (4a)$$

$$\mathbf{y}(k) = \mathbf{C}\mathbf{x}(k), \quad (4b)$$

with  $\mathbf{A} = \mathbf{e}^{\mathbf{F}T_s}$  and  $\mathbf{B} = -\mathbf{F}^{-1}(\mathbf{I}_4 - \mathbf{A})\mathbf{G}$ , since  $\mathbf{F}$  is nonsingular. Here,  $\mathbf{e}$  is the matrix exponential, and  $k \in \mathbb{N}$  denotes the discrete time step.

### III. OPTIMIZED PULSE PATTERNS

In this section the basic properties of OPPs are briefly explained. Moreover, the derivation of the stator current reference trajectory to be used in the MPC algorithm is presented.

#### A. Basic Properties

OPP enables the operation of a converter at very low switching frequencies with high quality output currents [5], [18]. As mentioned before, the optimization problem for the OPP calculation is designed such that it minimizes the THD of the stator current [8]. The result of this optimization procedure is a set of switching angles as a function of the modulation index which defines the OPP  $\mathbf{p}(d, m)$  as shown in Fig. 2(a). The notation  $\mathbf{p}(d, m)$  indicates that the OPP is a function of the pulse number  $d$ , i.e., the number of single-phase switching transitions and, consequently, switching angles in the first quarter of the fundamental period ( $\theta \in [0, 90^\circ]$ ), and modulation index  $m \in [0, 4/\pi]$ . Fig. 2(b) shows a single-phase two-level OPP, while the corresponding three-phase OPP is shown in Fig. 2(c). The latter is obtained by using quarter- and half-wave symmetry and further shifting the single-phase pattern by  $120^\circ$  and  $240^\circ$  for phases  $b$  and  $c$ , respectively.

#### B. Stator Current Trajectory

By applying an OPP to the inverter, the stator current with the lowest distortions is produced. Hence, the resulting current can be considered as a reference for the MPC algorithm presented in Section IV. Specifically, the stator current reference trajectory  $\mathbf{i}_{s,\text{ref}}$  is a combination of the fundamental  $\mathbf{i}_{s1,\text{ref}}$  and the harmonic  $\mathbf{i}_{sh,\text{ref}}$  component, i.e.,

$$\mathbf{i}_{s,\text{ref}} = \mathbf{i}_{s1,\text{ref}} + \mathbf{i}_{sh,\text{ref}}. \quad (5)$$

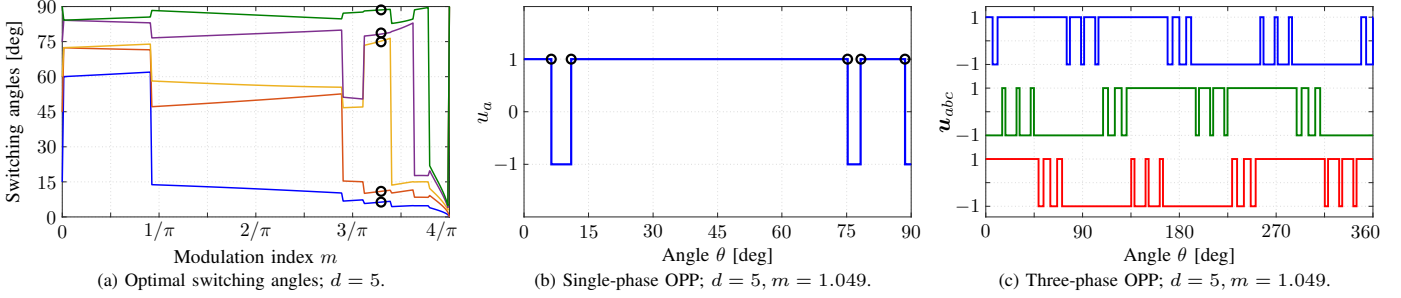


Fig. 2: Optimized pulse pattern (OPP)  $\mathbf{p}(d, m)$  for a two-level converter with  $d = 5$  switching angles per quarter of the fundamental period. The single- and three-phase pulse patterns correspond to the modulation index  $m = 1.049$ . The optimal switching angles for  $m = 1.049$  are indicated by (black) circles.

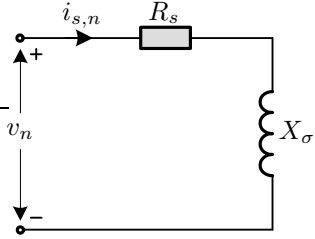


Fig. 3: Harmonic model of an induction machine in the p.u. system.

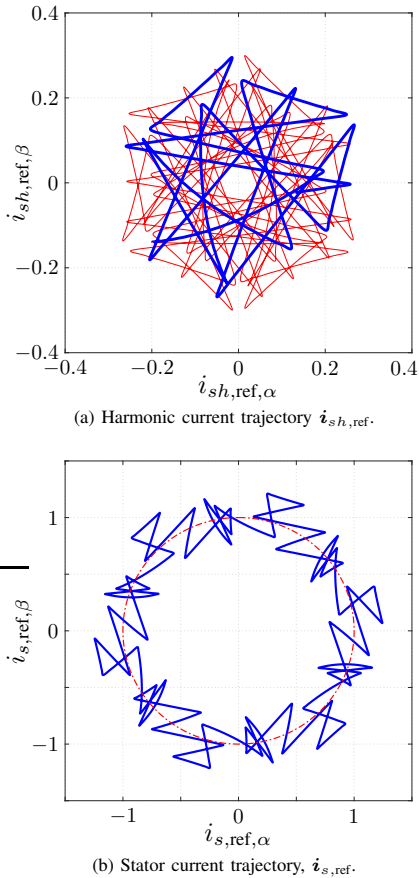


Fig. 4: Current reference trajectory for the OPP shown in Fig. 2. The blue line in (a) highlights  $\mathbf{i}_{sh,ref}$  for one-sixth of the fundamental period. The red (dash-dotted) line in (b) is the fundamental component  $\mathbf{i}_{s1,ref}$  of the stator current.

In (5), the fundamental component  $\mathbf{i}_{s1,ref}$  is produced by an outer loop, while the harmonic component  $\mathbf{i}_{sh,ref}$  can be computed by performing Fourier analysis on the OPP in use. To this end, the harmonic model of the induction machine

shown in Fig. 3 can be used, where  $X_\sigma = \Phi/x_r$  is the total leakage reactance. As shown in [5, Section 3.4], by neglecting the stator resistance, the current harmonics that result by applying the three-phase OPP  $\mathbf{u}_{abc}(\theta)$  are given by

$$\hat{i}_{s,n} = \frac{V_{dc}}{2X_\sigma} \frac{\hat{u}_n}{n\omega_1}, \quad (6)$$

where  $\hat{u}_n$  is the amplitude of the  $n^{\text{th}}$  voltage harmonic and  $\omega_1 = 2\pi f_1$  is the fundamental angular frequency. By performing the discrete Fourier transform of the switching pattern  $\mathbf{u}_{abc}(\theta)$ , the amplitudes  $\hat{u}_n$  and respective phases  $\hat{\phi}_n$  of the voltage harmonics are calculated. Therefore, the harmonic current component of the reference trajectory can be computed as

$$\mathbf{i}_{sh,ref}(\theta) = \sum_{n=5,7,\dots,N_h} \hat{i}_{sn} \sin(n\theta - \hat{\phi}_n), \quad (7)$$

where the harmonic order  $n$  is a non-triplen odd integer, and  $N_h$  the maximum harmonic number to be included in the current reference. It is worth mentioning that due to the fact that the harmonic current repeats every  $60^\circ$ , it is calculated only for one-sixth of the fundamental period. The complete harmonic current trajectory is formed by simply adding the other five  $60^\circ$  sections, each one rotated by  $60^\circ$  with respect to the previous section. To visualize this, Fig. 4(a) shows the harmonic current trajectory corresponding to the OPP in Fig. 2, with a  $60^\circ$  section highlighted for better insight. Finally, the calculated harmonic component is superimposed on the fundamental component according to (5) to generate the current reference trajectory  $\mathbf{i}_{s,ref}$  shown in Fig. 4(b).

#### IV. GRADIENT-BASED PREDICTIVE PULSE PATTERN CONTROL ALGORITHM

The basis of the proposed control approach lies in the combination of OPPs [8], [10] with gradient-based direct MPC [9], [19]. In doing so, excellent steady-state performance is achieved, while the slow dynamics associated to OPPs when used in a closed-loop setting are overcome. In the sequel of this section, the basic principles of the proposed control strategy are presented.

##### A. Control Problem

The objectives of the controller are twofold. At steady-state operation, accurate tracking of the stator current reference trajectory is required so that the resulting current has as low

harmonic distortions as possible. Moreover, during transients, the controller should exhibit fast dynamic responses with very short settling times.

To achieve the aforementioned control objectives, the controller is formulated as a constrained optimal problem with a receding horizon policy. A prediction horizon  $T_p$  of finite length is selected, and the goal is to modify the  $z \in \mathbb{N}$  switching time instants of the nominal OPP that fall within  $T_p$ , such that the rms error of the stator current is minimized. To this end, we introduce the vectors

$$\mathbf{t}_{\text{ref}} = [t_{1,\text{ref}} \ t_{2,\text{ref}} \ \dots \ t_{z,\text{ref}}]^T, \quad (8a)$$

$$\mathbf{U} = [\mathbf{u}_{abc}^T(t_0) \ \mathbf{u}_{abc}^T(t_{1,\text{ref}}) \ \dots \ \mathbf{u}_{abc}^T(t_{z,\text{ref}})]^T, \quad (8b)$$

$$\mathbf{t} = [t_1 \ t_2 \ \dots \ t_z]^T. \quad (8c)$$

where  $\mathbf{t}_{\text{ref}} \in \mathbb{R}^z$  is the vector of switching time instants of the nominal OPP within  $T_p$ ,  $\mathbf{U} \in \{-1, 1\}^{3(z+1)}$  is the vector of the corresponding OPP switch positions,<sup>2</sup> and  $\mathbf{t} \in \mathbb{R}^z$  includes the to-be-computed (i.e., modified) switching time instants.

Given the above, the objective function that takes into account the *weighted* (squared) rms error of the stator current and the changes in the switching time instants of the nominal OPP is

$$J = \frac{1}{T_p} \left( \int_0^{T_p} \|\dot{\mathbf{i}}_{s,\text{ref}}(t) - \dot{\mathbf{i}}_s(t)\|_2^2 dt \right) + \|\Delta \mathbf{t}\|_{\mathbf{R}}^2, \quad (9)$$

where the minimization of the current (rms) tracking error is equivalent to minimizing the THD of the stator current [9]. Moreover,  $\Delta \mathbf{t} = (\mathbf{t}_{\text{ref}} - \mathbf{t})$  are the (to-be-applied) modifications on the nominal OPP. Note that  $\mathbf{R}$  in (9) is a positive definite, diagonal matrix whose entries penalize the deviation of the computed switching time instants  $\mathbf{t}$  with respect to the nominal OPP switching time instants  $\mathbf{t}_{\text{ref}}$ .<sup>3</sup> Finally, it is worth pointing out that the prediction horizon consists of multiple subintervals, i.e.,  $[0, t_{1,\text{ref}})$ ,  $[t_{1,\text{ref}}, t_{2,\text{ref}})$ ,  $[t_{2,\text{ref}}, t_{3,\text{ref}})$ ,  $\dots$ , and  $[t_{z,\text{ref}}, T_p)$ .

As explained in [9] and [19], since function (9) is a cubic function of time, the associated control problem is nonconvex. To bring it into a convex form, a simplification is made in (9), namely, instead of accounting for the (weighted) rms error, the deviation only at the OPP switching time instants is penalized. Provided that the prediction horizon  $T_p$  is long enough to include at least two switching instants, this simplification estimates the rms error accurately enough. In doing so, the objective function becomes quadratic, i.e.,

$$J = \sum_{i=1}^z \|\dot{\mathbf{i}}_{s,\text{ref}}(t_{i,\text{ref}}) - \dot{\mathbf{i}}_s(t_{i,\text{ref}})\|_2^2 + \|\Delta \mathbf{t}\|_{\mathbf{R}}^2. \quad (10)$$

In a next step, function (10) has to be minimized for the sequence of OPP switch positions  $\mathbf{U}$ , as defined in (8b), to yield the modified switching time instants  $\mathbf{t}$ . To do so, the evolution of the stator current  $\dot{\mathbf{i}}_s$  within each subinterval of the prediction horizon has to be computed for each of the

<sup>2</sup>Note that the first entry of  $\mathbf{U}$  is the switch position applied at the end of the last sampling interval, i.e.,  $\mathbf{u}_{abc}(t_0^-)$ .

<sup>3</sup>The  $\|\xi\|_{\mathbf{R}}^2$  denotes the squared norm of a vector  $\xi$  weighted with the matrix  $\mathbf{R}$ .

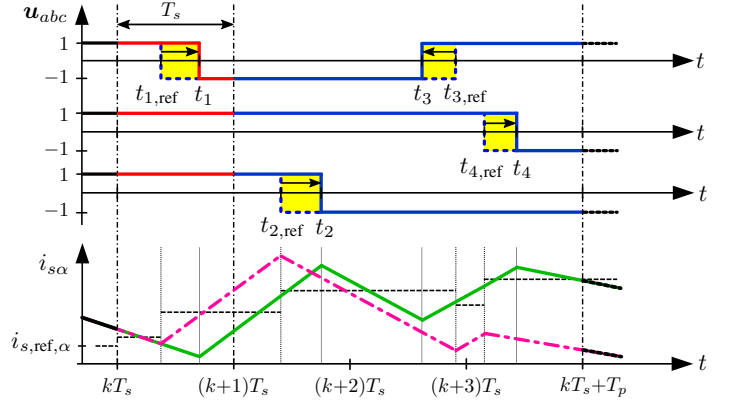


Fig. 5: Example of the evolution of one controlled variable (e.g., stator current  $i_{s\alpha}$ ) within a four-step ( $T_p = 4T_s$ ) prediction horizon by applying the depicted pulse pattern. Both the nominal OPP and the modifications introduced by the controller are shown. In the bottom figure, the dash-dotted (magenta) line represents the current (linearized) trajectory when applying the nominal OPP, while the solid (green) line shows the (linearized) current trajectory based on the modified pulse pattern.

OPP switch positions  $\mathbf{u}_{abc}$  within  $T_p$ . To simplify this task, and given that the prediction horizon  $T_p$  is small compared to the fundamental period  $T_1$ , i.e.,  $T_p \ll T_1$ , it is assumed that the stator current evolves linearly within each subinterval. Therefore, the stator current trajectories within the subintervals can be described by their corresponding gradients, i.e.,

$$\mathbf{m}(t_{i,\text{ref}}) = \frac{d\dot{\mathbf{i}}_s(t_{i,\text{ref}})}{dt} = \mathbf{C}(\mathbf{F}\mathbf{x}(t_{i,\text{ref}}) + \mathbf{G}\mathbf{u}_{abc}(t_{i,\text{ref}})), \quad (11)$$

where  $i \in \{0, 1, 2, \dots, z\}$ . Note that, as can be seen in (11), the gradients at the optimal OPP switching instants  $t_{1,\text{ref}}$ ,  $t_{2,\text{ref}}$ ,  $\dots$ ,  $t_{z,\text{ref}}$  depend on the respective state, i.e.,  $\mathbf{x}(t_{1,\text{ref}})$ ,  $\mathbf{x}(t_{2,\text{ref}})$ ,  $\dots$ ,  $\mathbf{x}(t_{z,\text{ref}})$ , respectively, to provide an as accurate computation of the corresponding gradient as possible.

As explained in [9], with (11), function (10) can be written in vector form as

$$J = \|\mathbf{r} - \mathbf{M}\mathbf{t}\|_2^2 + \|\Delta \mathbf{t}\|_{\mathbf{R}}^2, \quad (12)$$

where  $\mathbf{r} \in \mathbb{R}^{2z}$  depends on the reference values and measurements of the stator current, while the entries of  $\mathbf{M} \in \mathbb{R}^{2z \times z}$  depend on the slopes with which the stator current evolves within the prediction horizon. Both  $\mathbf{r}$  and  $\mathbf{M}$  are given in the appendix. For a better understanding, the following example is given.

**Example 1:** Consider the drive system in Fig. 1. As depicted in Fig. 5,  $\mathbf{u}_{abc}(t_0^-) = [1 \ 1 \ 1]^T$ , with  $t_0 \equiv kT_s$ , was applied at the end of the previous sampling interval. According to the illustrated OPP, four nominal switching time instants  $t_{1,\text{ref}}$ ,  $t_{2,\text{ref}}$ ,  $t_{3,\text{ref}}$ , and  $t_{4,\text{ref}}$ , with switch positions  $\mathbf{u}_{abc}(t_{1,\text{ref}})$ ,  $\mathbf{u}_{abc}(t_{2,\text{ref}})$ ,  $\mathbf{u}_{abc}(t_{3,\text{ref}})$ , and  $\mathbf{u}_{abc}(t_{4,\text{ref}})$ , respectively, fall within the prediction horizon  $T_p$ . The corresponding continuous-time evolution of one of the controlled variables, e.g.,  $i_{s\alpha}$  (dash-dotted, magenta line), is shown along with its sampled reference (dotted, black line). The stator current is assumed to evolve linearly with a constant slope within each subinterval.

## B. Optimal Control Algorithm

The block diagram of the proposed GP<sup>3</sup>C algorithm is shown in Fig. 6. Moreover, the pseudocode of the control



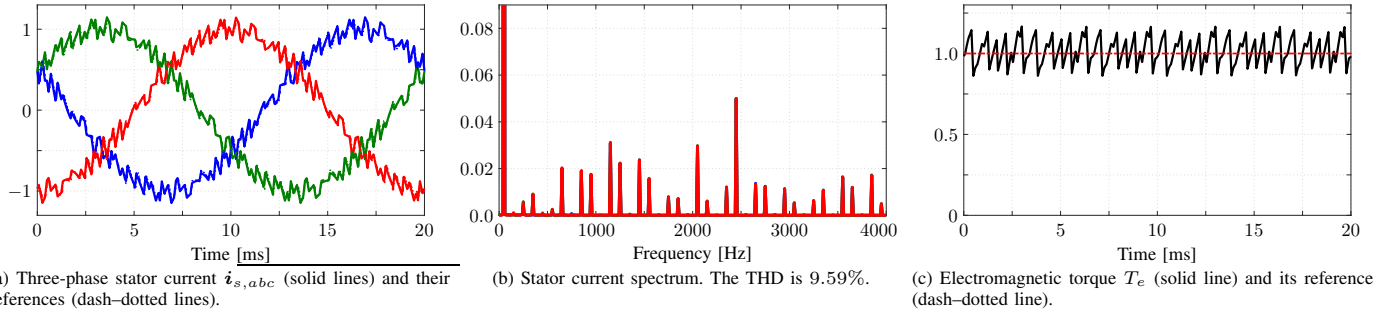


Fig. 7: Simulation results produced by the proposed GP<sup>3</sup>C algorithm at steady-state operation, nominal speed and rated torque. The modulation index is  $m = 1.049$ , the pulse number  $d = 10$ , and the switching frequency is 1050 Hz.

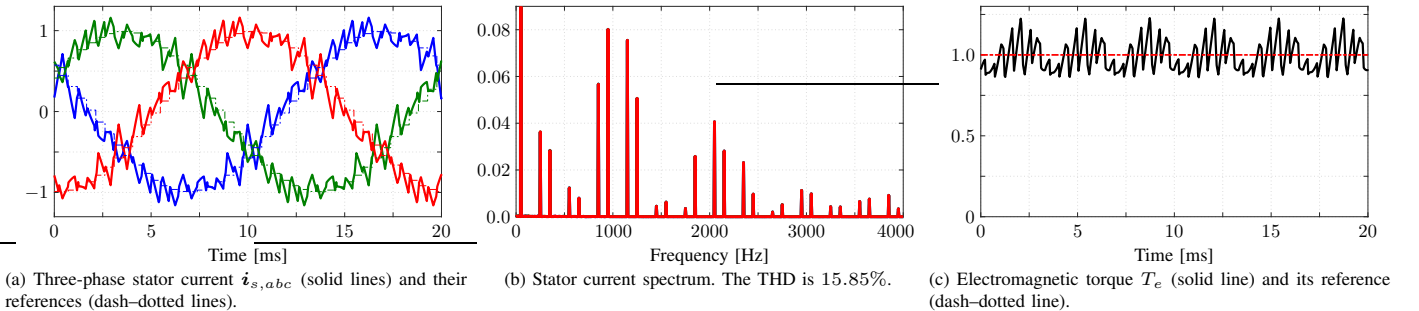


Fig. 8: Simulation results produced by FOC with SVM at steady-state operation, nominal speed and rated torque. The switching frequency is 1050 Hz.

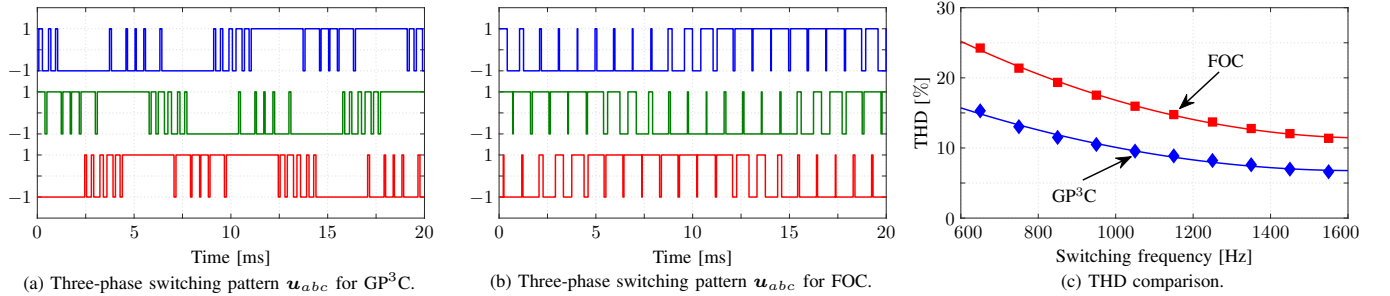


Fig. 9: The three-phase switching pattern during steady-state operation for (a) GP<sup>3</sup>C and (b) FOC with SVM. (c) The stator current THD as a function of the switching frequency for FOC with SVM and GP<sup>3</sup>C (operation at nominal speed and rated torque).

Finally, the horizon is shifted by one sampling interval and the whole procedure is recomputed over the shifted horizon based on new measurements and an updated OPP as per the receding horizon policy [5].

**Example 2:** Consider the pulse pattern  $\mathbf{U}$  over the prediction horizon shown in Fig. 5. The switching time instants  $t_{1,ref} - t_{4,ref}$  of the depicted part of the OPP are modified in such a manner that the error between the controlled variable (stator current) and its reference is minimized. The corresponding evolution of the stator current is shown in green, while the sampled reference is shown with a dotted, black line. The (modified) pattern that falls within the first sampling interval  $T_s$ —shown in red in Fig. 5—is applied to the inverter and the horizon is shifted by one  $T_s$ .

## V. PERFORMANCE EVALUATION

In this section, the performance of the proposed GP<sup>3</sup>C scheme is assessed for the drive system shown in Fig. 1 using simulations. The inverter is supplied by a six-pulse rectifier with an average dc-link voltage  $V_{dc} = 650$  V (voltage ripple peak-to-peak = 91.2 V). The squirrel-cage IM is rated

at 400 V rms line-to-line voltage, 4.4 A rms phase current, 3 kVA apparent power, 50 Hz nominal stator frequency and it has a total leakage reactance  $X_\sigma = 0.128$  p.u. The sampling interval is  $T_s = 50 \mu\text{s}$  and the prediction horizon  $N_p = 15$ . The OPP in use has a pulse number  $d = 10$ , i.e., the device switching frequency is 1050 Hz, while the modulation index is  $m = 1.049$ .

The steady-state performance of the drive is shown in Figs. 7 and 9(a), where operation at nominal speed and rated torque is considered. As can be seen in Fig. 7(a), the three-phase stator current waveforms—illustrated over one fundamental period—accurately track their references. The resulting current spectrum is shown in Fig. 7(b). Current harmonics are located at odd and non-triplen integer multiples of the fundamental frequency. The THD, which quantifies the current tracking performance of the controller, is 9.59%, i.e., it is low considering the switching frequency of 1050 Hz and the relatively low total leakage reactance. Fig. 7(c) shows the electromagnetic torque and Fig. 9(a) shows the three-phase switching pattern generated by the controller.

For comparison purposes, field oriented control (FOC) with

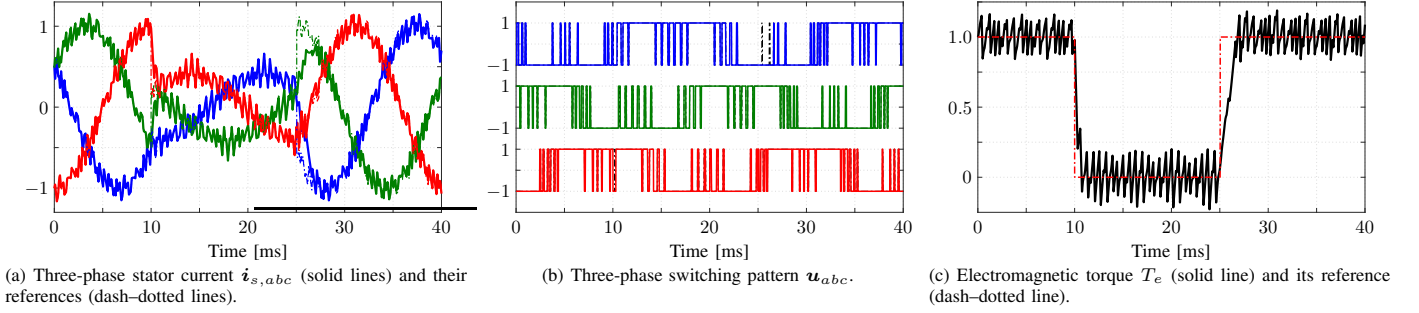


Fig. 10: Simulation results produced by the proposed  $GP^3C$  algorithm during torque reference steps. The pulse number is  $d = 10$  and switching frequency is 1050 Hz.

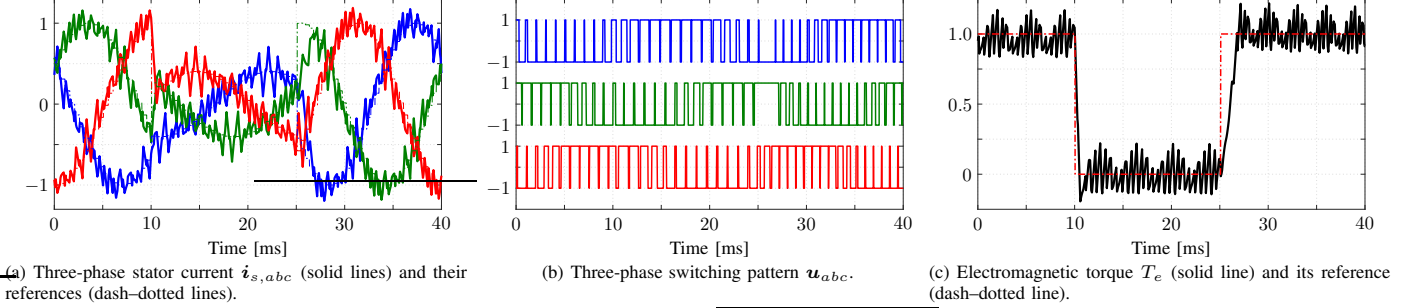


Fig. 11: Simulation results produced by FOC with SVM during torque reference steps. The switching frequency is 1050 Hz.

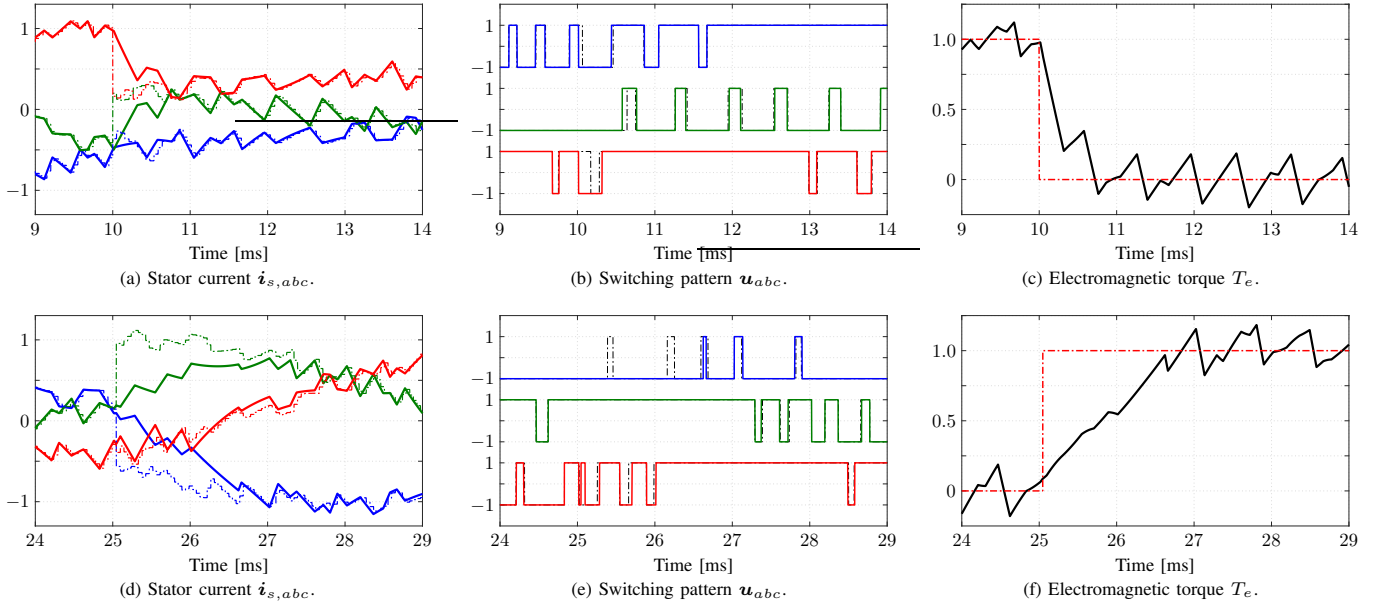


Fig. 12: Transient performance of  $GP^3C$  at rated speed during a torque reference (a)–(c) step-down change, and (d)–(f) step-up change. In (b) and (e), the (black) dash-dotted lines refer to the switching sequence of the unmodified, nominal OPP, whereas the solid lines correspond to the modified switching sequence as computed by  $GP^3C$ .

space vector modulation (SVM) is also implemented. The switching frequency is the same as that of  $GP^3C$ , i.e., 1050 Hz, and the proportional-integral (PI) controllers of FOC are tuned using the modulus optimum method. The waveforms generated by FOC are shown in Figs. 8 and 9(b). From the stator current waveform in Fig. 8(a), it is readily apparent that FOC has significantly higher current ripple compared to  $GP^3C$ . Correspondingly, the harmonic components in the current spectrum (see Fig. 8(b)) are higher, particularly the 5<sup>th</sup>, 7<sup>th</sup>, and sideband harmonics around the switching frequency. The 5<sup>th</sup> and 7<sup>th</sup> harmonics are pronounced due to the fact that the dc-link contains a voltage ripple of 300 Hz. Moreover, the current

THD of 15.85% is clearly worse than that of  $GP^3C$ .

Finally, to further highlight the benefits of  $GP^3C$  during steady state, Fig. 9(c) compares its performance with that of FOC in terms of current THD over a wide range of switching frequencies. As can be inferred, to achieve a current THD of about 11.6%, FOC requires a switching frequency of at least 1500 Hz, whereas  $GP^3C$  requires only 850 Hz. Hence,  $GP^3C$  allows for a reduction of the switching frequency by 43%. Consequently, the switching power losses can be significantly reduced, resulting in an increase in the overall efficiency of the drive system. It can be concluded that  $GP^3C$  (in comparison to FOC) effectively reduces the current distortions

by almost 40%, while also rejecting the adverse effect of the low frequency dc-link voltage ripple.

Figs. 10 and 11 compare the performance of the two control schemes during transients. While operating at nominal speed, reference torque steps of magnitude 1 p.u. are imposed, and the reference torque is translated into the corresponding stator current reference. As can be seen in Fig. 10(a), the stator currents accurately track their new reference values without any overshoot/undershoot, resulting in a good torque reference tracking, see Fig. 10(c). On the contrary, FOC suffers a visible undershoot in the torque as shown in Fig. 11. As expected, the dynamic performance of the modulator-based, linear control scheme is slightly slower than that of the MPC-based strategy.

The transient performance of GP<sup>3</sup>C is shown in more detail in Fig. 12. When applying the torque step-down, a phase-shift of  $-6.77^\circ$  is introduced into the nominal OPP, which is equivalent to shifting the nominal OPP by 0.3761 ms forward in time. To track the references, additional volt-second contributions are required from the three-phases. As shown in Fig. 12(b), GP<sup>3</sup>C achieves this by shortening the pulses in phases *a* and *c*, and lengthening the pulse in phase *b*. The resulting torque settling time is less than 2 ms. Similar behavior is observed during the torque reference step-up change. As can be observed, the proposed controller inherits the favorable dynamic behavior of MPC by appropriately modifying the nominal OPP to remove the torque error as quickly as possible.

## VI. CONCLUSIONS

This paper proposed an MPC scheme, called GP<sup>3</sup>C, for a low-voltage drive that employs OPPs. As shown, the proposed controller has two features, namely, optimal performance during steady state, i.e., minimal current THD for a given switching frequency, and very short settling times during transients. To do so, principles of constrained optimal control are employed that enable the controller to modify the OPP in an optimal manner in real time. Moreover, the adoption of a receding horizon policy provides GP<sup>3</sup>C with the ability to achieve superior dynamic performance during transients. Thanks to these characteristics, GP<sup>3</sup>C can outperform conventional control solutions, such as FOC with SVM.

## APPENDIX

The vector  $\mathbf{r}$  and matrix  $\mathbf{M}$  in (10) are

$$\mathbf{r} = \begin{bmatrix} \mathbf{i}_{s,\text{ref}}(t_1) - \mathbf{i}_s(t_0) \\ \mathbf{i}_{s,\text{ref}}(t_2) - \mathbf{i}_s(t_0) \\ \mathbf{i}_{s,\text{ref}}(t_3) - \mathbf{i}_s(t_0) \\ \vdots \\ \mathbf{i}_{s,\text{ref}}(t_z) - \mathbf{i}_s(t_0) \end{bmatrix}$$

and

$$\mathbf{M} = \begin{bmatrix} \mathbf{m}_{t_0} & \mathbf{0}_2 & \mathbf{0}_2 & \dots & \mathbf{0}_2 \\ \mathbf{m}_0 & \mathbf{m}_{t_1} & \mathbf{0}_2 & \dots & \mathbf{0}_2 \\ \mathbf{m}_0 & \mathbf{m}_1 & \mathbf{m}_{t_2} & \dots & \mathbf{0}_2 \\ \vdots & \vdots & \vdots & \ddots & \vdots \\ \mathbf{m}_0 & \mathbf{m}_1 & \mathbf{m}_2 & \dots & \mathbf{m}_{t_{z-1}} \\ \mathbf{m}_0 & \mathbf{m}_1 & \mathbf{m}_2 & \dots & \mathbf{m}_{z-1} \end{bmatrix}$$

with

$$\begin{aligned} \mathbf{m}_{t_\ell} &= \mathbf{m}(t_{\ell,\text{ref}}) \\ \mathbf{m}_\ell &= \mathbf{m}(t_{\ell,\text{ref}}) - \mathbf{m}(t_{\ell+1,\text{ref}}) \end{aligned}$$

where  $\ell \in \{0, 1, 2, \dots, z-1\}$ .

## REFERENCES

- [1] J. B. Rawlings and D. Q. Mayne, *Model Predictive Control: Theory and Design*. Madison, WI, USA: Nob Hill, 2009.
- [2] P. Cortés, M. P. Kazmierkowski, R. M. Kennel, D. E. Quevedo, and J. Rodríguez, "Predictive control in power electronics and drives," *IEEE Trans. Ind. Electron.*, vol. 55, no. 12, pp. 4312–4324, Dec. 2008.
- [3] J. Rodríguez, M. P. Kazmierkowski, J. R. Espinoza, P. Zanchetta, H. Abu-Rub, H. A. Young, and C. A. Rojas, "State of the art of finite control set model predictive control in power electronics," *IEEE Trans. Ind. Informat.*, vol. 9, no. 2, pp. 1003–1016, Oct. 2012.
- [4] P. Karamanakos, E. Liegmann, T. Geyer, and R. Kennel, "Model predictive control of power electronic systems: Methods, results, and challenges," *IEEE Open J. Ind. Appl.*, vol. 1, pp. 95–114, 2020.
- [5] T. Geyer, *Model Predictive Control of High Power Converters and Industrial Drives*. Hoboken, NJ, USA: Wiley, 2016.
- [6] P. Karamanakos and T. Geyer, "Guidelines for the design of finite control set model predictive controllers," *IEEE Trans. Power Electron.*, vol. 35, no. 7, pp. 7434–7450, Jul. 2020.
- [7] S. Mariéthoz, A. Domahidi, and M. Morari, "High-bandwidth explicit model predictive control of electrical drives," *IEEE Trans. Ind. Appl.*, vol. 48, no. 6, pp. 1980–1992, Nov./Dec. 2012.
- [8] G. S. Buja, "Optimum output waveforms in PWM inverters," *IEEE Trans. Ind. Appl.*, vol. IA-16, no. 6, pp. 830–836, Nov./Dec. 1980.
- [9] P. Karamanakos, R. Mattila, and T. Geyer, "Fixed switching frequency direct model predictive control based on output current gradients," in *Proc. IEEE Ind. Electron. Conf.*, Washington, D.C., USA, Oct. 2018, pp. 2329–2334.
- [10] G. S. Buja and G. B. Indri, "Optimal Pulsewidth Modulation for Feeding AC Motors," *IEEE Trans. Ind. Appl.*, vol. IA-13, no. 1, pp. 38–44, Jan. 1977.
- [11] J. Holtz and B. Beyer, "Optimal synchronous pulsewidth modulation with a trajectory-tracking scheme for high-dynamic performance," *IEEE Trans. Ind. Appl.*, vol. 29, no. 6, pp. 1098–1105, Nov./Dec. 1993.
- [12] —, "Fast current trajectory tracking control based on synchronous optimal pulsewidth modulation," *IEEE Trans. Ind. Appl.*, vol. 31, no. 5, pp. 1110–1120, Sep./Oct. 1995.
- [13] J. Holtz and N. Oikonomou, "Synchronous optimal pulsewidth modulation and stator flux trajectory control for medium-voltage drives," *IEEE Trans. Ind. Appl.*, vol. 43, no. 2, pp. 600–608, Mar./Apr. 2007.
- [14] T. Geyer, N. Oikonomou, G. Papafiotiou, and F. D. Kieferndorf, "Model predictive pulse pattern control," *IEEE Trans. Ind. Appl.*, vol. 48, no. 2, pp. 663–676, Mar./Apr. 2012.
- [15] N. Oikonomou, C. Gutscher, P. Karamanakos, F. D. Kieferndorf, and T. Geyer, "Model predictive pulse pattern control for the five-level active neutral-point-clamped inverter," *IEEE Trans. Ind. Appl.*, vol. 49, no. 6, pp. 2583–2592, Nov./Dec. 2013.
- [16] I. Takahashi and T. Noguchi, "A new quick-response and high-efficiency control strategy of an induction motor," *IEEE Trans. Ind. Appl.*, vol. IA-22, no. 5, pp. 820–827, Sep. 1986.
- [17] J. Holtz, "The representation of ac machine dynamics by complex signal flow graphs," *IEEE Trans. Ind. Electron.*, vol. 42, no. 3, pp. 263–271, Jun. 1995.
- [18] A. K. Rathore, J. Holtz, and T. Boller, "Synchronous optimal pulsewidth modulation for low-switching-frequency control of medium-voltage multilevel inverters," *IEEE Trans. Ind. Electron.*, vol. 57, no. 7, pp. 2374–2381, Jul. 2010.
- [19] P. Karamanakos, M. Nahalparvari, and T. Geyer, "Fixed switching frequency direct model predictive control with continuous and discontinuous modulation for grid-tied converters with *LC*L filters," *IEEE Trans. Control Sys. Technol.*, vol. 29, no. 4, pp. 1503–1518, Jul. 2021.